Theor Chem Acc (2009) 124:345–354
DOI 10.1007/s00214-009-0618-9

REGULAR ARTICLE

Structure, stability and electronic property of the gold-doped germanium clusters: $AuGe_n$ (n = 2–13)

Xiao-Jun Li · Ke-He Su

Received: 31 May 2009 / Accepted: 27 July 2009 / Published online: 14 August 2009

Abstract The structure, stability and electronic property of the $AuGe_n$ (n = 2–13) clusters with different spin configurations are systematically investigated with density-functional theory approach at UB3LYP/LanL2DZ level. In examining the lowest energy structures, it is found that the growth behaviors for the small-sized $AuGe_n$ (n = 2–9) clusters and relatively large-sized $AuGe_n$ (n = 10–13) clusters are different. As the number of Ge atom increases, the Au atom would gradually move from convex to surface and to interior sites. For the most stable structures of $AuGe_n$ (n = 10–13) clusters, the Au atom would be completely surrounded by the Ge atoms to form Au-encapsulated Ge_n cages. Natural population analysis shows that the charges always transfer from the Au atom to the Ge_n framework except for the $AuGe_2$ cluster. This indicates that the Au atom acts as electron donor even the 5d orbitals of the Au atom are not significantly involved in chemical bonding. The analyses of the average atomic binding energies as well as the dissociation energies and the second-order differences of total energy show that the $AuGe_n$ clusters with n = 5, 9 and 12 are more stable than their neighboring ones, in which the bicapped pentagonal prism $AuGe_{12}$ in D_{2d} symmetry is most stable. The highest occupied molecular orbital–lowest unoccupied molecular orbital gaps are explored to be in the region of semiconductors and the more stable clusters have slightly smaller gaps. It could be expected that the stable clusters might be considered as the novel building blocks in practical applications, e.g., the cluster-assembled semiconductors or optoelectronic material.

Keywords $AuGe_n$ cluster · Structure · Stability · Electronic property · DFT

X.-J. Li · K.-H. Su (✉)
School of Natural and Applied Sciences,
Northwestern Polytechnical University,
Xi'an, Shaanxi 710072,
People's Republic of China
e-mail: sukehe@nwpu.edu.cn

X.-J. Li
Department of Chemistry and Chemical Engineering,
Weinan Teachers University,
Weinan, Shaanxi 714000,
People's Republic of China

1 Introduction

The semiconductor clusters with transition metal (TM) impurities have attracted great interest for cluster-assembled optoelectronic materials and the development of new species in nanoscale applications [1–13]. Their properties can be changed by the size of the clusters, the shape of the equilibrium geometries and the property of the doped TM atom. It is interesting that germanium and silicon are isovalent, but their chemical properties are quite different. Previous calculations also indicated that the threshold number of germanium clusters with the first-row TM (TM = Fe, Mn, Ni, Cu and Zn) [14–18] and the third-row W [19] impurities appears at n = 10 other than that of some silicon clusters [2–7]. In addition, the TM-doped germanium clusters exhibit many novel properties such as the sized selectivity, the highest occupied molecular orbital (HOMO)–lowest unoccupied molecular orbital (LUMO) gap, different charge-transfer direction and the magnetic property [14–22]. A proper HOMO–LUMO gap value (i.e., less than 2 eV) could be expected that the stable TM-doped germanium clusters might be considered as the novel building blocks in practical applications, e.g., the cluster-

assembled semiconductors or optoelectronic material. Therefore, theoretical and experimental investigations on the TM-doped germanium clusters have been carried out. Zhao and Wang [15] investigated the geometries, stabilities and magnetic properties of $MnGe_n$ ($n = 2$–16) clusters using the generalized gradient approximation. They found that the magnetic moment of the Mn atom does not quench when the Mn atom is embedded in all sized Ge_n ($n = 2$–16) clusters. In contrast to the Zn-doped germanium clusters in which the 12 Ge containing icosahedral $ZnGe_{12}$ is the lowest energy structure [18], the TM-doped (TM = Ni, Cu or Co) Ge_{10} clusters [16, 17, 20] are the most stable clusters. Zhang et al. [23] prepared the Co/Ge binary clusters with laser vaporization and observed a remarkably strong signal of $[CoGe_{10}]^-$ in the mass spectrum. Kumar et al. [24–26] reported the encapsulated large-sized caged $TMGe_n$ ($n = 8$–12, 14–16) theoretically using the ab initio pseudopotential plane wave method. The results show that the most strikingly doping of X_{12} (X = Ge and Sn) with Mn leads to an icosahedral super atom with a high magnetic moment of 5 μ_B [24, 25]. The similar large HOMO–LUMO gaps and weak interactions of these clusters make such species attractive for cluster-assembled materials [26].

The third-row gold atom has $5s^25p^65d^{10}6s^1$ electron configuration in the outer space. Its electronegativity and electron affinity are also quite large. These features manifest that the relativistic effects contract and stabilize the s and p shells while expand and destabilize the d and all f shells [27]. Therefore, the bimetallic gold clusters have been found fascinating physical properties such as optical, electronic and magnetic properties [28–33]. Obviously, it is very interesting to explore the chemical and physical properties of the Au-doped germanium clusters. As far as we are aware, the investigation on the Au-doped germanium clusters has not been reported. In this paper, a detailed investigation was carried out with DFT-UB3LYP/LanL2DZ method on the structure, relative stability, HOMO–LUMO gap, charge transfer and natural electron configuration of the Au-doped germanium clusters.

2 Theoretical methods

The structures of the $AuGe_n$ ($n = 2$–13) clusters with different spin configurations are optimized with the density-functional theory using the spin unrestricted B3LYP exchange-correlation functionals [34–39], i.e., Lee–Yang–Parr correlation functional [36] in conjunction with a hybrid exchange functional [37]. The double-ζ LanL2DZ [40–42] basis set is chosen because it provides an effective core potential (ECP) to consider the relativistic effects of the heavy TM atom and to reduce the number of the two-electron integrals. The Au atom is treated with a 19 electronic ECP of $5s^25p^65d^{10}6s^1$ in the valence space. This method is chosen because it has been proven to be suitable for the geometry, stability and electronic properties of the $TM@Ge_n$ clusters [17–19, 21]. Additional computational results on the bond lengths, harmonic vibrational frequencies and the dissociation energies of the specific Ge_2, AuGe and Au_2 molecules obtained with B3LYP/LanL2DZ would be compared to assess the method.

The structures of the low-lying isomers of $AuGe_n$ ($n = 2$–13) clusters are searched extensively based on the information of the previously optimized Ge_n or $CuGe_n$ clusters in Ref. [17, 43] by placing a Au atom at different adsorption or substitutional sites. The stationary structure is determined with harmonic vibrational frequency analyses. If an imaginary frequency is found, a relaxation along the coordinates of the imaginary vibrational mode is carried out until the real local minimum is reached. Thus, the isomers for a given n in the $AuGe_n$ clusters are the local minima. The relative stability of the $AuGe_n$ isomers also for a given n is determined with the total energy of the molecules.

All theoretical calculations are performed with the Gaussian-03 package [44]. The default numerical integration grid (75,302) is generally applied. In a few cases, the fine grid (99,590) is used to check the suspicious results. It turns out that the fine grid is sometimes important for the $AuGe_n$ clusters.

3 Results and discussion

3.1 Comparison of the results of diatomic Ge and Au compounds

The bond lengths, harmonic vibrational frequencies and the dissociation energies of Ge_2, AuGe and Au_2 molecules are listed in Table 1. The ground state of AuGe is an open shell $5d^{10}\sigma^2\sigma^2\pi$ configuration with $^2\Pi$ electronic state formed through the interaction of $Ge(4s^2p^2)$ and $Au(5d^{10}6s^1)$. Table 1 shows that all the calculated results of the Ge_2, AuGe and Au_2 molecules are in agreement with the experimental and other theoretical results [17, 45–55]. The equilibrium bond lengths have deviations within 1–6%. The harmonic frequency of Ge_2 is lower than the experimental values by 24 cm^{-1} [47] or 36 ± 5 cm^{-1} [48, 49] and that of AuGe is 42.7 cm^{-1} [52, 53] lower. The reason might be that the B3LYP approach may predict slightly longer bond lengths and smaller harmonic vibrational frequencies [56]. The theoretical dissociation energies are slightly lower than the experiments [47–50, 52, 53, 55] by about 0.4 eV. Therefore, the calculations are acceptable for predicting the properties of $AuGe_n$ ($n = 2$–13) clusters.

Table 1 Bond length (R in Å), harmonic vibrational frequency (F in cm^{-1}) and dissociation energy (D_e in eV) for the ground state of the diatomic Au and Ge molecules

Molecule	Method	State	R	F	D_e
Ge_2	B3LYP/LanL2DZ	$^3\Sigma_g^-$	2.53	250	2.34
			2.55 [17]		
	B3LYP/DZP++ [45]	$^3\Sigma_g^-$	2.41	277	2.87
	MRCI [46]	$^3\Sigma_g^-$	2.42	270	2.70 ± 0.07
	Experiment			274 [47]	2.65 [47]
				286 ± 5 [48, 49]	2.70 ± 0.07 [48, 49]
					2.82 (D_0^0) [50]
GeAu	B3LYP/LanL2DZ	$^2\Pi$	2.46	207	2.40
	DFT SP [51]	$^2\Pi$	2.38		3.14
	Experiment [52]	$^2\Pi$	2.38	249.7	2.83
				249.7 [53]	
Au_2	B3LYP/LanL2DZ [54]	$^1\Sigma_g^+$	2.51	192	1.85
	MRSDCI [53]	$^1\Sigma_g^+$	2.56		
	Experiment [50]	$^1\Sigma_g^+$	2.4719	190.9	2.30 (D_0^0)
					2.33 [55]

3.2 Structure and stability of $AuGe_n$ ($n = 2$–9) clusters

All the calculations show that the lowest energy Au-doped germanium clusters are in doublet states. The equilibrium geometries of $AuGe_n$ ($n = 2$–9) clusters are shown in Fig. 1. It is shown in the figure that $AuGe_2$ could be in a triangular and two linear structures. The symmetric triangular structure in C_{2v} group with $^2B_1$ state is more stable by 0.86 eV than the non-symmetric (in C_s) triangular structure with $^4A''$ state. The $^2A_1$ and $^4A_2$ states in C_{2v} symmetry are 0.18 and 1.16 eV higher in energy compared with the ground state, respectively. The respective energies obtained with time-dependent TD-B3LYP/LanL2DZ are 0.23 and 1.42 eV, which are consistent with the results of the direct calculations by altering the occupied and unoccupied orbitals. The linear $C_{\infty v}$ isomers with different spins are found to be unstable with imaginary frequencies. Therefore, the most stable $AuGe_2$ cluster is the symmetric triangle isomer (2a, shown in Fig. 1) in $^2B_1$ state. The structure can also be regarded as the Au atom directly caps on the Ge_2 cluster or substituting of the central Ge atom in the Ge_3 cluster. This result is consistent with that of the doublet $CuGe_2$ [17] cluster.

For the $AuGe_3$ cluster, three stable structures are examined. The Ge–Ge–Ge bond angle (95.6°) of the rhombic 3a isomer, generated from Au atom being capped on the Ge_3 cluster, is very close to that of the Ge_3 structure. The 3b isomer is a distorted Y-type structure, which can be described as one Ge atom being bonded on the apical Ge atom in the lowest energy $AuGe_2$ cluster. If one Ge atom is capped on the lowest energy $AuGe_2$ cluster, the bent rhombic 3c isomer may be formed. When comparing these three isomers, the rhombic 3a is most stable. It is shown that the rhombic isomer with $^2A_1$ state is slightly lower in energy than the identical structure with $^2B_2$ state by 0.15 eV. The total energies of the spin quartet and sextet states of different geometries are higher than those with doublet spin configurations. Therefore, the lowest energy structure of $AuGe_3$ displays C_{2v} symmetry with $^2A_1$ state. Although the structure of the lowest energy $AuGe_3$ is different from those of $MnGe_3$ [15] and WGe_3 [19] clusters (in C_{3v} symmetry), it is similar to those of $TMGe_3$ (TM = Ni, Cu, Zn and Co) [16–18, 20].

The lowest energy structure of $AuGe_4$ is a distorted pyramid isomer (4a in Fig. 1) in C_s symmetry with $^2A'$ electronic state. This structure can be viewed as a Ge atom capped on the face of the most stable $AuGe_3$ cluster. A five-member ring 4b isomer, which can be regarded as a Au atom being bonded into one edge of the nearly coplanar Ge_4 square, is also a low energy structure lying only 0.12 eV above the 4a isomer. The 4c and 4d isomers are obviously higher in energy than the lowest energy structure 4a by 0.44 and 0.51 eV, respectively. Interestingly, the $AuGe_4$ 4d isomer has a higher symmetry which can be formed by substituting the apical Ge atom in the Ge_5 (D_{3h}) isomer with an Au atom. The structure of the most stable $AuGe_4$ predicted in this work is similar to those of WGe_4 [19] and $CoGe_4$ [20] clusters, but differs from those of $TMGe_4$ (TM = Mn, Ni, Cu and Zn) [15–18] clusters.

Referring the equilibrium geometries of the lowest energy Ge_6 [17] and $AuGe_4$ cluster mentioned above, four kinds of $AuGe_5$ isomers can be found. The face-capped trigonal bipyramidal 5a isomer can be regarded as the apical Ge atom in the Ge_6 cluster being substituted by Au

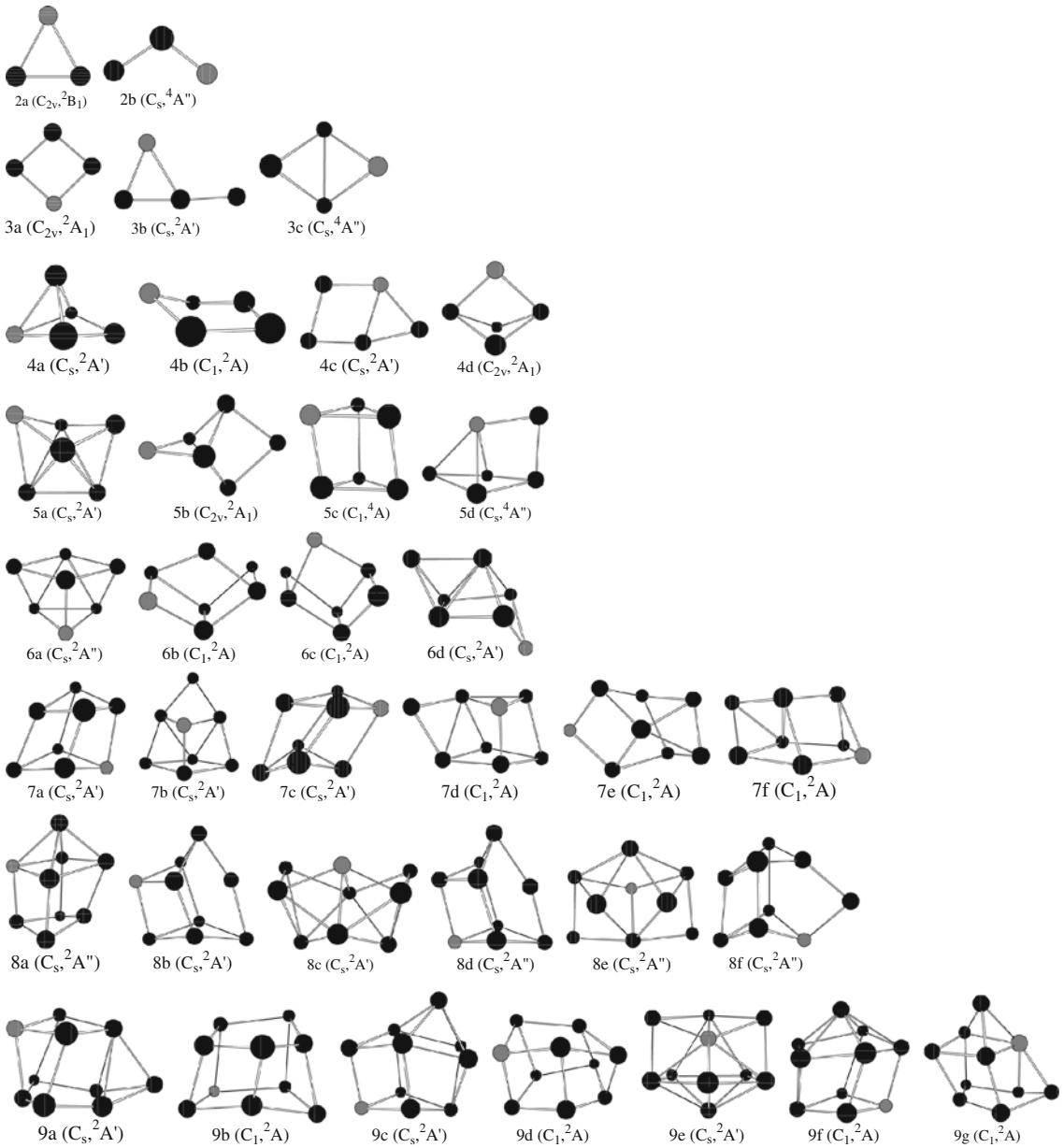

Fig. 1 The equilibrium geometries of $AuGe_n$ (n = 2–9) clusters. *Gray and black* represent the Au and Ge atoms, respectively. According to their energy ordering, the isomers are labeled as *n*a, *n*b and *n*c etc., and the *n*a correspond to the lowest energy isomer

atom. Similarly, the edge-capped trigonal bipyramidal 5b isomer may be formed. Although the 5a and 5b isomers can be generated from the same precursory molecule, their energies are different. Table 2 lists the energy differences. It is indicated that the face-capped trigonal bipyramidal 5a isomer is more stable in energy than the edge-capped 5b isomer by 0.23 eV. Both the triangular prism 5c and the 5d isomers are less stable than the face-capped 5a isomer by 1.05 and 1.15 eV, respectively. Therefore, the 5a isomer in C_s symmetry with $^2A'$ state is the lowest-energy structure. When compared with the most stable $TMGe_5$ [15–20] clusters, the $AuGe_5$ 5a isomer is close to $NiGe_5$ [16] and $CuGe_5$ [17], but it is different from those with TM = Mn, Zn, W and Co [15, 18–20].

Geometries of four possible $AuGe_6$ clusters are optimized when a Ge atom at different site in the low-lying Ge_7 cluster of 7b in Ref. [17] is substituted by an Au atom. The structure of the lowest energy $AuGe_6$ displays a C_s symmetry with $^2A''$ electronic state as shown in Fig. 1 (6a). The relative energies for 6b, 6c and 6d are 0.29, 0.33 and 0.41 eV, respectively. The structure of the most stable $AuGe_6$ is close to that of the $CuGe_6$ [17] cluster, but differs from those of $TMGe_6$ (TM = Mn, Ni, Zn, W and Co) [15, 16, 18–20]. It should be pointed out that the pentagonal

Table 2 Symmetry (Sym), electronic state (State), the lowest harmonic vibrational frequency (F in cm^{-1}), the shortest Au-Ge and Ge-Ge bond length (in Å), total energy (E_T in hartree), and relative energy (ΔE in eV) for the $AuGe_n$ ($n = 2$–9) clusters

Cluster	Sym	State	F	Au-Ge	Ge-Ge	E_T	ΔE
$AuGe_2$	C_{2v}(a)	$^2B_1$	100.1	2.668	2.542	−142.9942086	0.00
	C_s(b)	$^4A''$	41.5	2.470	2.551	−142.9625421	0.86
$AuGe_3$	C_{2v}(a)	$^2A_1$	51.5	2.537	2.484	−146.7779078	0.00
	C_s(b)	$^2A'$	17.9	2.573	2.416	−146.7585844	0.53
	C_s(c)	$^4A''$	35.1	2.690	2.676	−146.7370031	1.11
$AuGe_4$	C_s(a)	$^2A'$	56.0	2.757	2.598	−150.5553643	0.00
	C_1(b)	^2A	32.9	2.568	2.431	−150.5508888	0.12
	C_s(c)	$^2A'$	40.9	2.554	2.444	−150.5393782	0.44
	C_{2v}(d)	$^2A_1$	41.0	2.703	2.627	−150.5364912	0.51
$AuGe_5$	C_s(a)	$^2A'$	37.9	2.604	2.495	−154.3566859	0.00
	C_{2v}(b)	$^2A_1$	32.5	2.624	2.534	−154.3482327	0.23
	C_1(c)	^4A	21.6	2.563	2.619	−154.3180299	1.05
	C_s(d)	$^4A''$	36.1	2.572	2.626	−154.3142771	1.15
$AuGe_6$	C_s(a)	$^2A''$	39.9	2.588	2.710	−158.1428816	0.00
	C_1(b)	^2A	31.1	2.585	2.604	−158.1321245	0.29
	C_1(c)	^2A	31.8	2.599	2.590	−158.1308951	0.33
	C_s(d)	$^2A'$	15.8	2.574	2.607	−158.1279583	0.41
$AuGe_7$	C_s(a)	$^2A'$	44.1	2.619	2.635	−161.9269706	0.00
	C_s(b)	$^2A'$	38.0	2.558	2.592	−161.9186506	0.23
	C_s(c)	$^2A'$	35.3	2.610	2.580	−161.9151097	0.32
	C_1(d)	^2A	33.9	2.574	2.536	−161.9109831	0.44
	C_1(e)	^2A	12.3	2.592	2.611	−161.9083118	0.51
	C_1(f)	^2A	34.3	2.651	2.608	−161.9007862	0.71
$AuGe_8$	C_s(a)	$^2A''$	3.7	2.552	2.613	−165.7016061	0.00
	C_s(b)	$^2A'$	42.9	2.658	2.549	−165.7002672	0.04
	C_s(c)	$^2A'$	40.0	2.644	2.601	−165.6975963	0.11
	C_s(d)	$^2A''$	41.3	2.596	2.477	−165.6915361	0.27
	C_s(e)	$^2A''$	27.4	2.599	2.568	−165.6902541	0.31
	C_s(f)	$^2A''$	34.2	2.636	2.518	−165.6886195	0.35
$AuGe_9$	C_s(a)	$^2A'$	38.3	2.613	2.509	−169.4933044	0.00
	C_1(b)	^2A	30.9	2.631	2.611	−169.4908116	0.07
	C_s(c)	$^2A'$	27.5	2.603	2.616	−169.4832902	0.27
	C_1(d)	^2A	31.3	2.574	2.607	−169.4827287	0.29
	C_s(e)	$^2A'$	32.1	2.576	2.762	−169.4806290	0.34
	C_1(f)	^2A	33.3	2.576	2.732	−169.4795891	0.37
	C_1(g)	^2A	26.4	2.682	2.554	−169.4784676	0.40

bipyramid $AuGe_6$, which could be generated from the Au substitution of one equatorial Ge atom in the lowest energy Ge_7 (D_{5h}) cluster, is an unstable structure from our calculations.

The most stable $AuGe_7$ cluster is the distorted cubic prism $AuGe_7$ 7a isomer, which can be generated from two Ge atoms being symmetrically capped on the lowest energy $AuGe_5$ or one Ge atom being symmetrically capped on the lowest energy $AuGe_6$. It displays C_s symmetry with $^2A'$ electronic state. A less stable state $^2A''$ of the structure lying 0.15 eV above the ground state is also found. The 7b, 7c, 7d, 7e and 7f isomers have higher energies compared with the 7a structure in its ground state by 0.23, 0.32, 0.44, 0.51 and 0.71 eV, respectively. It is interesting that the lowest energy $AuGe_n$ cluster may not be obtained directly by adding an Au atom at any site of the lowest energy Ge_n clusters. Although the structure of the most stable $AuGe_7$ is different from those of $TMGe_7$ (TM = Mn, Ni, Cu and Co) [15–17, 20], it is similar to those of the $ZnGe_7$ [18] and WGe_7 [19] clusters.

For $AuGe_8$, the most stable structure is a capped square prism (8a) in C_s symmetry with $^2A''$ electronic state, which is similar to that of the $CuGe_8$ [17] cluster. Its formation could be a Ge atom capped on the bottom face of the lowest energy $AuGe_7$ or the apical Ge atom in the lowest energy Ge_9 being substituted by an Au atom. Other possible isomers (8b–8f) have energies higher than 8a by 0.04, 0.11, 0.27, 0.31 and 0.35 eV as shown in Table 2. Especially, the 8b isomer is slightly higher in energy than 8a by only 0.04 eV. Although both $AuGe_8$ 8b and 8d isomers are close in structure (i.e., the lowest energy $AuGe_7$ cluster being capped on the midst of the side arris by a Ge atom), they have different energies due to different states $^2A'$ and $^2A''$.

Twenty-six stable structures were obtained in $AuGe_9$ and the seven most stable isomers are listed in Fig. 1 (9a–9g). The lowest energy isomer is in C_s symmetry, a multi-rhombus prism with two side-capped Ge atoms (9a), which can be viewed as two Ge atoms capped on the lowest energy $AuGe_7$ cluster. This structure is different from those of $TMGe_9$ (TM = Fe, Ni, Cu, Zn, W and Co) [14, 16–20], in which the structures were found with very high energies or unstable when the TM atom is substituted with an Au atom. Other low-lying structures of $AuGe_9$ are the distorted pentagonal prism (9b) and typical multi-rhombus cages (9c, 9d, 9e, 9f and 9g). The relative energies are 0.07, 0.27, 0.29, 0.34, 0.37 and 0.40 eV, respectively.

3.3 Structure and stability of $AuGe_n$ ($n = 10$–13) clusters

The equilibrium geometries of $AuGe_n$ ($n = 10$–13) clusters are shown in Fig. 2. Similar to the formation of the previously examined $TMGe_{10}$ (TM = Fe, Mn and Zn) [14, 15, 18] cages, the Au-encapsulated cages are formed in the $AuGe_n$ ($n = 10$–13) clusters. For $AuGe_{10}$, the lowest energy structure is a C_{2v}-symmetrical pentagonal prism (10a) with $^2B_2$ electronic state. The Au atom is completely encapsulated into the inside of the pentagonal prism. The structure of pentagonal prism is the same as that in $FeGe_{10}$ cluster [14] but differs from those of $TMGe_{10}$ (TM = Mn, Ni, Cu, Zn, W and Co) [15–20] clusters. The 10b isomer

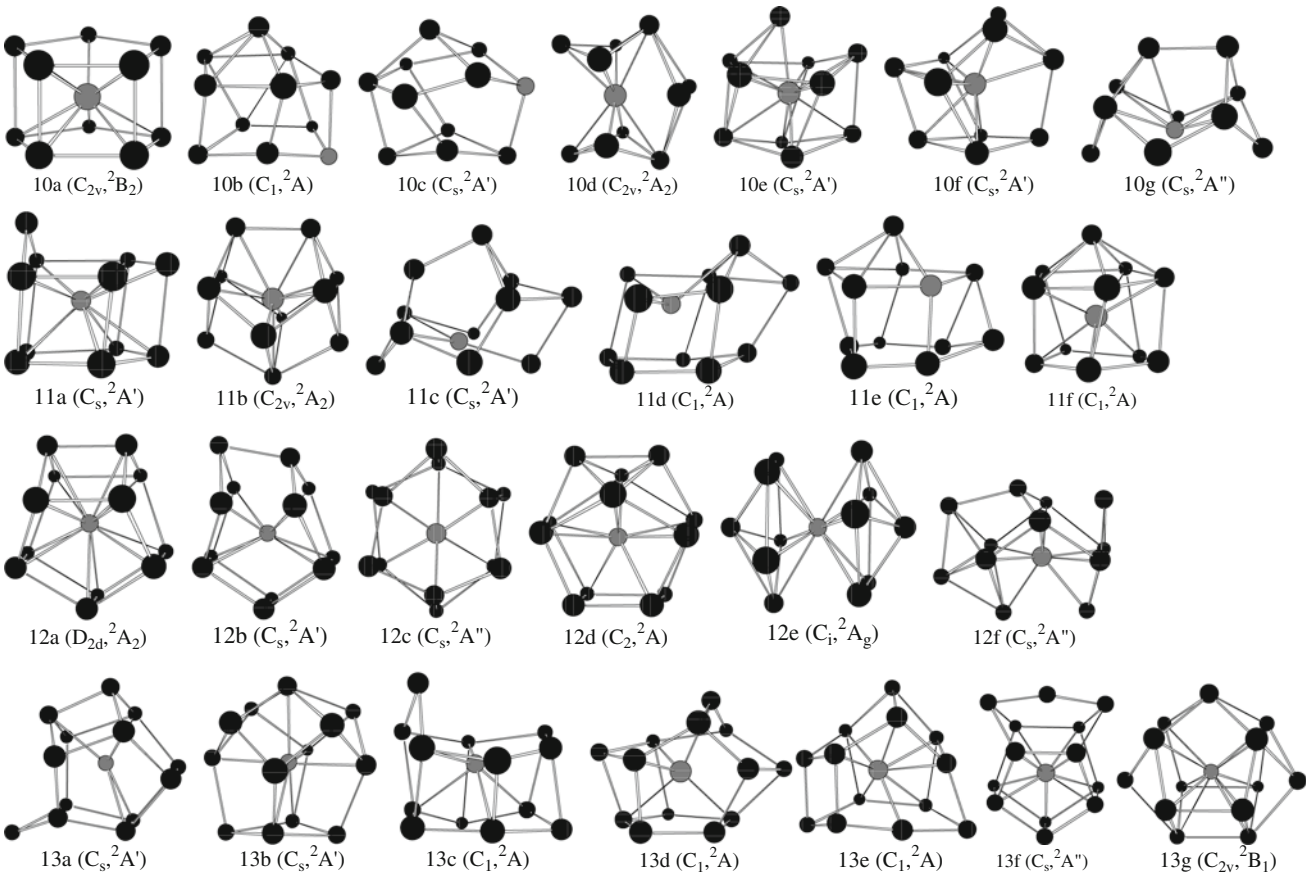

Fig. 2 The equilibrium geometries of $AuGe_n$ (n = 10–13) clusters. *Gray and black* represent the Au and Ge atoms, respectively. According to their energy ordering, the isomers are labeled as *n*a, *n*b and *n*c etc., and the *n*a correspond to the lowest energy isomer

can be interpreted as one Ge atom being capped on the top of the structure of $AuGe_9$ 9b. Its energy is 0.12 eV higher than that of the lowest energy structure (10a). Other Au-encapsulated cages, 9c, 9d, 9e, 9f and 9g, have higher energies by 0.20, 0.21, 0.25, 0.27 and 0.28 eV, respectively (Table 3).

Six $AuGe_{11}$ isomers can be optimized. The most stable $AuGe_{11}$ (11a) isomer with C_s symmetry in $^2A'$ state can be generated by capping a Ge atom on the side face of the pentagonal prism $AuGe_{10}$. However, it is very close in energy to the C_{2v}-symmetrical 11b isomer by 0.03 eV higher. Other structures generated by substituting the TM atom in the previously examined $TMGe_{11}$ (TM = Mn, Ni, Cu, Zn, W and Co) [15–20] clusters with an Au atom are considered. The energies for 11c–11f are higher than that of the 11a isomer by 0.14, 0.31, 0.33 and 0.39 eV, respectively. The structure of the lowest energy $AuGe_{11}$ is different from those of $TMGe_{11}$ (TM = Fe, Mn, Ni, Cu, Zn, W and Co) [14–20].

For $AuGe_{12}$, the bicapped pentagonal prism 12a is optimized to be the lowest energy structure, which displays a higher D_{2d} symmetry with $^2A_2$ state. Similar to the lowest energy $AuGe_{12}$ structure, the low-lying 12b isomer can be generated by capping two Ge atoms on the side face of the pentagonal prism $AuGe_{10}$, but its energy is higher than that of the lowest energy $AuGe_{12}$ by 0.32 eV. Referring the structures of the $TMGe_{12}$ (TM = Fe, Mn, Cu, Zn, W and Co) [14, 15, 17–20] clusters, we optimized the geometries of $AuGe_{12}$ clusters. A hexagonal prism 12c, a multipentagonal 12d and 12e–12f isomers are located at the minima, but their energies are higher by 0.40, 0.72, 0.96 and 1.22 eV, respectively. The structure in an isomer of $NiGe_{12}$ [16] or $CoSi_{12}$ [8] cluster was found to be similar to the lowest energy $AuGe_{12}$. This result indicates that the TM-doped germanium clusters might have different growth behavior depended on the different TM atom and the number of Ge atoms. An icosahedral $ZnGe_{12}$ has been reported to have a stronger relative stability [18], but the icosahedral $AuGe_{12}$ was optimized to be an unstable structure with an imaginary vibrational frequency. Its stable structure, 12e, was finally found in C_i symmetry lying 0.96 eV higher in energy than the lowest energy 12a isomer.

If one Ge atom can be capped on the side face of the lowest energy $AuGe_{12}$, the most stable 13a isomer of $AuGe_{13}$ in C_s symmetry with $^2A'$ state is obtained. Other

Table 3 Symmetry (Sym), electronic state (State), the lowest harmonic vibrational frequency (F in cm^{-1}), the shortest Au-Ge and Ge-Ge bond length (in Å), total energy (E_T in hartree), and relative energy (ΔE in eV) for the $AuGe_n$ (n = 10–13) clusters

Cluster	Sym	State	F	Au-Ge	Ge-Ge	E_T	ΔE
$AuGe_{10}$	C_{2v}(a)	$^2B_2$	15.1	2.715	2.670	−173.2742605	0.00
	C_1(b)	^2A	33.6	2.634	2.536	−173.2699013	0.12
	C_s(c)	$^2A'$	24.3	2.584	2.601	−173.2668495	0.20
	C_{2v}(d)	$^2A_2$	18.1	2.641	2.792	−173.2664510	0.21
	C_s(e)	$^2A'$	4.5	2.657	2.836	−173.2651159	0.25
	C_s(f)	$^2A'$	4.6	2.687	2.682	−173.2644131	0.27
	C_s(g)	$^2A''$	21.6	2.788	2.563	−173.2637957	0.28
$AuGe_{11}$	C_s(a)	$^2A'$	41.7	2.779	2.590	−177.0597504	0.00
	C_{2v}(b)	$^2A_2$	12.1	2.752	2.704	−177.0587546	0.03
	C_s(c)	$^2A'$	19.6	2.831	2.568	−177.0547774	0.14
	C_1(d)	^2A	33.8	2.752	2.567	−177.0482303	0.31
	C_1(e)	^2A	37.1	2.682	2.536	−177.0477388	0.33
	C_1(f)	^2A	17.0	2.673	2.665	−177.0453398	0.39
$AuGe_{12}$	D_{2d}(a)	$^2A_2$	43.4	2.865	2.574	−180.8664091	0.00
	C_s(b)	$^2A'$	15.1	2.795	2.564	−180.8545576	0.32
	C_s(c)	$^2A''$	35.6	2.639	2.624	−180.8518564	0.40
	C_2(d)	^2A	14.0	2.804	2.655	−180.8398662	0.72
	C_i(e)	^2A_g	20.9	2.853	2.826	−180.8309700	0.96
	C_s(f)	$^2A''$	21.2	2.662	2.627	−180.8215218	1.22
$AuGe_{13}$	C_s(a)	$^2A'$	39.5	2.796	2.579	−184.6432605	0.00
	C_s(b)	$^2A'$	14.6	2.790	2.591	−184.6408047	0.07
	C_1(c)	^2A	38.5	2.675	2.536	−184.6337266	0.26
	C_1(d)	^2A	19.3	2.726	2.598	−184.6273246	0.43
	C_1(e)	^2A	32.0	2.706	2.517	−184.6235794	0.54
	C_s(f)	$^2A''$	29.9	2.756	2.542	−184.6149572	0.77
	C_{2v}(g)	$^2B_1$	32.9	2.834	2.725	−184.6125887	0.83

isomers, 13b–13g, have energies higher than the 13a structure by 0.07, 0.26, 0.43, 0.54, 0.77 and 0.83 eV, respectively. It is interesting that the isomer 13g with the highest energy has the highest symmetry (C_{2v}) in the isomers of $AuGe_{13}$.

Obviously, the growth behavior for the small-sized $AuGe_n$ (n = 2–9) clusters is different from the relatively large-sized $AuGe_n$ (n = 10–13) clusters. The most significant behavior is that the position of the Au atom in the lowest energy $AuGe_n$ clusters gradually moves from convex to surface and to interior sites as the number of Ge atom increases from 2 to 13. The Au atom fully falls into the inside of the Ge_n frame to form an encapsulated cage in the relative large-size clusters starting from $AuGe_{10}$. This is in good agreement with the previously investigated $TMGe_{10}$ (TM = Fe, Mn and Zn) [14, 15, 18] clusters, but differs from the TM-doped germanium clusters with TM = Ni, Cu, W and Co [16, 17, 19, 20].

3.4 Relative stability of different sized $AuGe_n$ clusters

It should be very important to discuss the relative stability of different sized $AuGe_n$ (n = 2–13) clusters because the species are attractive for novel cluster-assembled optoelectronic materials. The relative stability of different sized $AuGe_n$ clusters can be represented with the average atomic binding energy, the dissociation energy and the second-order difference of the total energy. These results are shown in Figs. 3, 4 and 5.

The average atomic binding energy (E_b), the dissociation energy (D_e) and the second-order difference of the total energy ($\Delta_2 E$) for different sized $AuGe_n$ clusters are defined as follows

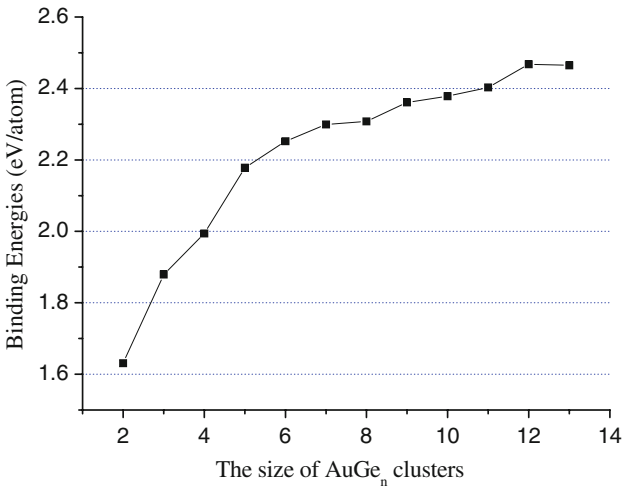

Fig. 3 Sized dependence of the average atomic binding energies of $AuGe_n$ (n = 2–13) clusters

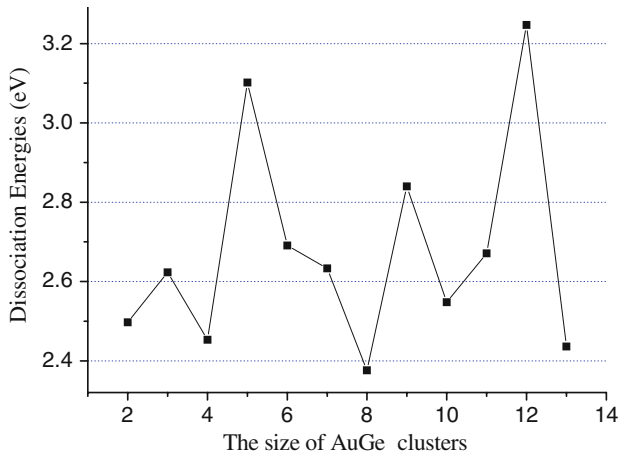

Fig. 4 Sized dependence of the dissociation energies of $AuGe_n$ (n = 2–13) clusters

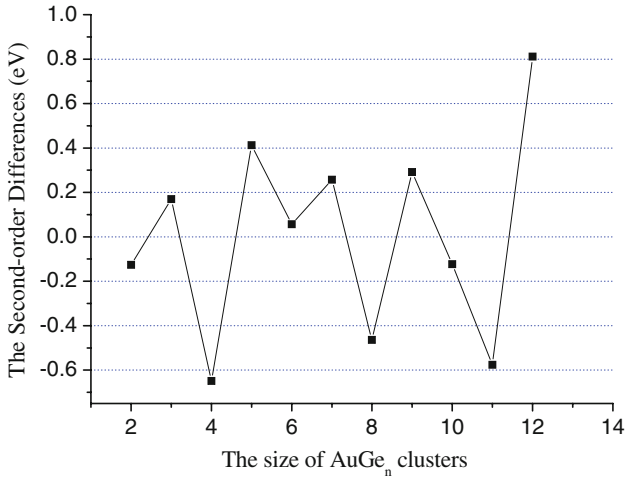

Fig. 5 Sized dependence of the second-order differences of $AuGe_n$ ($n = 2$–13) clusters

$$E_b(n) = [E_T(Au) + nE_T(Ge) - E_T(AuGe_n)]/(n+1)$$

$$D_e(n) = E_T(AuGe_{n-1}) + E_T(Ge) - E_T(AuGe_n)$$

$$\Delta_2E(n) = E_T(AuGe_{n+1}) + E_T(AuGe_{n-1}) - 2E_T(AuGe_n)$$

where $E_T(Au)$, $E_T(Ge)$, $E_T(AuGe_n)$, $E_T(AuGe_{n-1})$ and $E_T(AuGe_{n+1})$ represent the total energies of Au, Ge and the lowest energies of $AuGe_n$, $AuGe_{n-1}$ and $AuGe_{n+1}$ clusters, respectively.

Figure 3 shows that the average atomic binding energy of the $AuGe_n$ clusters dramatically increases with the size $n \leq 6$ and increases smoothly with the size $n = 7$–12. This trend is due to that the number of dangling bonds of Ge atoms in the large-sized $AuGe_n$ clusters is less than that of the relatively small-sized clusters and the average atomic binding energy gradually increases along with the increasing number of Ge atom. However, the average atomic binding energy of the $AuGe_{13}$ cluster is slightly lower than that of the $AuGe_{12}$ cluster by 0.003 eV. Hence, the peak of the average atomic binding energy is at $n = 12$. The dissociation energy D_e and the second-order difference Δ_2E are sensitive quantities that can also reflect the relative stability of the $AuGe_n$ clusters. Especially, the Δ_2E might be directly compared with the relative abundances of the mass spectroscopy experiments. As shown in Fig. 4, the local maxima of the dissociation energy D_e of the $AuGe_n$ clusters appear at 3, 5, 9 and 12, which differ from those of $NiGe_n$ [16] and $CuGe_n$ [17] clusters. It is also found that the $AuGe_5$, $AuGe_9$ and $AuGe_{12}$ clusters have higher Ge dissociation energies, indicating that these clusters are more stable than their neighboring ones. The relatively high stability is mainly associated with the geometry and the number of dangling bonds in these clusters. In the case of the sealed $AuGe_{12}$ cluster, which has a higher D_{2d} symmetry, the dangling bonds are almost eliminated by the encapsulated Au atom. Therefore, the bicapped pentagonal prism $AuGe_{12}$ is the most stable cluster. Figure 5 shows that the peaks of the Δ_2E for the $AuGe_n$ clusters appear at $n = 3$, 5, 7, 9 and 12, which is almost in agreement with those in the D_e curves. Therefore, these clusters are also more stable than their neighbors. These stable clusters are also similar to $MnGe_n$ [15]. In particular, the highest E_b, D_e or Δ_2E of the investigated clusters is in $AuGe_{12}$, which is similar to that in $TiSi_{12}$ [2] and $ZnGe_{12}$ [18] clusters.

3.5 HOMO–LUMO gap

Table 4 illustrates the HOMO–LUMO gaps of the lowest energy $AuGe_n$ ($n = 2$–13) clusters. It is shown that the gaps, 1.028–1.296 eV, in the large-sized clusters with

Table 4 HOMO-LUMO gap (in eV), natural charge population, and natural electron configuration of the lowest energy $AuGe_n$ ($n = 2$–13) clusters

Cluster	HOMO-LUMO gap	Natural population on Au atom	Natural electron configuration on Au atom				
			6s	5d	6p	7s	6d
$AuGe_2$	1.502	−0.031	1.14	9.86	0.03		
$AuGe_3$	1.642	0.079	1.07	9.80	0.05		
$AuGe_4$	1.672	0.124	0.99	9.83	0.05		0.01
$AuGe_5$	1.664	0.170	0.95	9.82	0.05		0.01
$AuGe_6$	1.503	0.158	0.97	9.82	0.05		0.01
$AuGe_7$	1.358	0.171	0.98	9.80	0.05		0.01
$AuGe_8$	1.238	0.266	0.87	9.80	0.07		0.01
$AuGe_9$	1.296	0.202	0.94	9.80	0.05		0.01
$AuGe_{10}$	1.150	0.128	0.81	9.78	0.26	0.01	0.02
$AuGe_{11}$	1.256	0.165	0.81	9.77	0.23	0.01	0.01
$AuGe_{12}$	1.028	0.185	0.81	9.76	0.23	0.01	0.01
$AuGe_{13}$	1.264	0.195	0.81	9.77	0.22	0.01	0.01

$n \geq 8$ are smaller than those, 1.358–1.672 eV, in the small-sized ones. This property is similar to that in the $TMGe_n$ (TM = Cu and Co) [17, 20] clusters. It is also found that the gaps are obviously lower than those, 1.637–2.963 eV, of the corresponding Ge_n ($n = 3$–13) [17] clusters. The HOMO–LUMO gap values are in the typical magnitude (i.e., less than 2 eV) of semiconductors. Therefore, it could be expected that the stable $AuGe_n$ clusters might be considered as the novel building blocks in practical applications, e.g., the cluster-assembled semiconductors or optoelectronic material.

3.6 Natural population analysis and charge transfer

A natural population analysis is able to find the charge transfer in a molecule. The results for the lowest energy $AuGe_n$ species are listed in Table 4. It is shown that different charge transfer appear in different sized clusters. For $AuGe_2$, the charge transfers slightly from the Ge atoms onto the Au atom. However, the transfer direction is reversed for the larger size $AuGe_n$ ($n = 3$–13) clusters, where the Au atom acts as an electron donor. The natural electron configuration on the Au atom shows that the natural population of 5d orbitals is about 9.8 indicating these orbitals are not significantly involved in chemical bonding. Natural populations of 6s and 6p orbitals of the Au atom are obviously different for the size of $n < 10$ and $n \geq 10$. This is due to the encapsulated cage appears for $n \geq 10$ and the charge transfers mainly from 6s to 6p orbitals. The charge transfer of the $AuGe_n$ ($n = 3$–13) clusters is similar to that of $TMGe_n$ (TM = Fe, Mn, Cu and Zn) [14, 15, 17, 18] but differs from that of the $TMGe_n$ (TM = Ni and W) [16, 19] clusters. For example, the charge in the WGe_n clusters always transfers from the Ge_n framework to the W atom [19]. However, the charge in $NiGe_n$ ($n \leq 6$ and $n \geq 12$) transfers from the Ni atom to the Ge_n framework and in reversed direction in $NiGe_n$ ($7 \leq n \leq 11$) [16].

4 Conclusions

The structure, stability and electronic property of the $AuGe_n$ ($n = 2$–13) clusters are systematically investigated at UB3LYP level of theory by employing the ECP LanL2DZ basis sets. The results are summarized as follows.

(1) The lowest energy structure in each of the $AuGe_n$ ($n = 2$–13) clusters was obtained. It is found that the growth behavior for the most stable small-sized $AuGe_n$ ($n = 2$–9) clusters is different from the relatively large-sized $AuGe_n$ ($n = 10$–13) ones. The Au atom moves gradually from convex to surface and to interior sites as the number of Ge atom increases from 2 to 13. The Au atom completely falls into the inside of the Ge_n frame to form an encapsulated cage starting from $AuGe_{10}$. The TM-doped germanium clusters might have different growth behavior depended on the different TM atom and the number of Ge atoms.

(2) The $AuGe_n$ clusters with $n = 5$, 9 and 12 are more stable than their neighboring ones according to the average atomic binding energy, the dissociation energy and the second-order difference of total energy. Especially, the bicapped pentagonal prism $AuGe_{12}$ is the most stable cluster, which is similar to the $TiSi_{12}$ and $ZnGe_{12}$ clusters.

(3) The HOMO–LUMO gaps in the large-sized clusters with $n \geq 8$ are smaller than those in the small-sized ones. The gaps of different $AuGe_n$ clusters are obviously lower than those of the corresponding Ge_n ($n = 3$–13) clusters. The gap values are in the typical region of semiconductors. Therefore, the stable $AuGe_n$ clusters could be expected to be the novel building blocks in practical applications, e.g., the cluster-assembled semiconductors or optoelectronic material.

(4) Natural population analysis shows that the charge always transfers from the Au atom to the Ge_n framework in the $AuGe_n$ ($n = 3$–13) clusters indicating that the Au atom acts as an electron donor. However, the Au atom in the $AuGe_2$ cluster acts as a very weak electron acceptor with slightly negative charge. It is also found that the natural population of 5d orbitals of the Au atom in the $AuGe_n$ ($n = 2$–13) clusters is about 9.8 indicating that these orbitals are not significantly involved in chemical bonding.

References

1. Torres MB, Fernandez EM, Balbas LC (2007) Phys Rev B 75:205425
2. Guo LJ, Liu X, Zhao GF, Luo YH (2007) J Chem Phys 126:234704
3. Kawamura H, Kumar V, Kawazoe Y (2004) Phys Rev B 70:245433
4. Chuang FC, Hsieh YY, Hsu CC, Albao MA (2007) J Chem Phys 127:144313
5. Peng Q, Shen JJ (2008) J Chem Phys 128:084711
6. Ma L, Zhao JJ, Wang JG, Lu QL, Zhu LZ, Wang GH (2005) Chem Phys Lett 411:279
7. Wang J, Ma QM, Xie Z, Liu Y, Li YC (2007) Phys Rev B 76:035406
8. Wang JG, Zhao JJ, Ma L, Wang BL, Wang GH (2007) Phys Lett A 367:335
9. Zhao WJ, Yang Z, Yan YL, Lei XL, Ge GX, Wang QL, Luo YH (2007) Acta Phys Sin 56:2596

10. Ma L, Zhao JJ, Wang JG, Wang BL, Lu QL, Wang GH (2006) Phys Rev B 73:125439
11. Hou XJ, Gopakumar G, Lievens P, Nguyen MT (2007) J Phys Chem A 111:13544
12. Han JG, Hagelberg F (2009) J Comput Theory Nanosci 6:257
13. Han JG, Xiao CY, Hagelberg F (2002) Struct Chem 13:173
14. Zhao WJ, Wang YX (2008) Chem Phys 352:291
15. Zhao WJ, Wang YX (2009) J Mol Struct (Theochem) 901:18
16. Wang J, Han JG (2006) J Phys Chem B 110:7820
17. Wang J, Han JG (2005) J Chem Phys 123:244303
18. Wang J, Han JG (2007) Chem Phys 342:253
19. Wang J, Han JG (2006) J Phys Chem A 110:12670
20. Jing Q, Tian FY, Wang YX (2008) J Chem Phys 128:124319
21. Wang J, Han JG (2008) J Phys Chem A 112:3224
22. Lu J, Nagase S (2003) Chem Phys Lett 372:394
23. Zhang X, Li GL, Gao Z (2001) Rapid Commun Mass Spectrom 15:1573
24. Kumar V, Kawazoe Y (2003) Appl Phys Lett 83:2677
25. Kumar V, Singh AK, Kawazoe Y (2004) Nano Lett 4:677
26. Kumar V, Kawazoe Y (2002) Phys Rev Lett 88:235504
27. Pyykkö P (1988) Chem Rev 88:563
28. Bishes GA, Morse MD (1991) J Chem Phys 95:5646
29. Negishi Y, Nakamura Y, Nakajima A, Kaya K (2001) J Chem Phys 115:3657
30. Bonačić-Koutecký V, Burda J, Mitrić R, Ge M, Zampella G, Fantucci P (2002) J Chem Phys 117:3120
31. Yuan DW, Wang Y, Zeng Z (2005) J Chem Phys 122:114310
32. Zorriasatein S, Joshi K, Kanhere DG (2008) J Chem Phys 128:184314
33. Fa W, Dong JM (2008) J Chem Phys 128:144307
34. Becke AD (1986) J Chem Phys 84:4524
35. Becke AD (1988) J Chem Phys 88:2547
36. Lee C, Yang W, Parr RG (1988) Phys Rev B 37:785
37. Becke AD (1988) J Chem Phys 88:1053
38. Becke AD (1993) J Chem Phys 98:5648
39. Kohn W, Sham LJ (1965) Phys Rev A 140:1133
40. Hay PJ, Wadt WR (1985) J Chem Phys 82:270
41. Wadt WR, Hay PJ (1985) J Chem Phys 82:284
42. Hay PJ, Wadt WR (1985) J Chem Phys 82:299
43. Zhao LZ, Lu WC, Wei Q, Zang QJ, Wang CZ, Ho KM (2008) Chem Phys Lett 455:225
44. Gaussian 03, Revision B.01, Frisch MJ, Trucks GW, Schlegel HB, Scuseria GE, Robb MA, Cheeseman JR, Montgomery JA Jr, Vreven T, Kudin KN, Burant JC, Millam JM, Iyengar SS, Tomasi J, Barone V, Mennucci B, Cossi M, Scalmani G, Rega N, Petersson GA, Nakatsuji H, Hada M, Ehara M, Toyota K, Fukuda R, Hasegawa J, Ishida M, Nakajima T, Honda Y, Kitao O, Nakai H, Klene M, Li X, Knox JE, Hratchian HP, Cross JB, Adamo C, Jaramillo J, Gomperts R, Stratmann RE, Yazyev O, Austin AJ, Cammi R, Pomelli C, Ochterski J, Ayala WPY, Morokuma K, Voth GA, Salvador P, Dannenberg JJ, Zakrzewski VG, Dapprich S, Daniels AD, Strain MC, Farkas O, Malick DK, Rabuck AD, Raghavachari K, Foresman JB, Ortiz JV, Cui Q, Baboul AG, Clifford S, Cioslowski J, Stefanov BB, Liu G, Liashenko A, Piskorz P, Komaromi I, Martin RL, Fox DJ, Keith T, Al-Laham MA, Peng CY, Nanayakkara A, Challacombe M, Gill PMW, Johnson B, Chen W, Wong MW, Gonzalez C, Pople JA (2003) Gaussian Inc., Pittsburgh
45. Xu WG, Zhao J, Li QS, Xie YM, Schaefer HFIII (2004) Mol Phys 102:579
46. Shim I, Sai Baba M, Gingerich KA (2002) Chem Phys 277:9
47. Arnold CC, Xu C, Burton GR, Neumark DM (1995) J Chem Phys 102:6982
48. Burton GR, Xu C, Neumark DM (1996) Surf Rev Lett 3:383
49. Burton GR, Xu C, Arnold CC, Neumark DM (1996) J Chem Phys 104:2757
50. Huber KP, Herzberg G (1979) Constants of diatomic molecules. Van Nostrand Reinhold, New York
51. Pershina V, Anton J, Fricke B (2007) J Chem Phys 127:134310
52. Kingcade JE Jr, Choudary UV, Gingerich KA (1979) Inorg Chem 18:3094
53. Balasubramanian K, Liao MZ (1987) J Chem Phys 86:5587
54. Guo JJ, Yang JX, Die D (2008) Phys B 403:4033
55. Lide DR (ed in Chief) (1996–1997) CRC handbook of chemistry and physics, 77th edn. CRC, Boca Raton
56. Zhang PX, Zhao YF, Hao FY, Song XD, Zhang GH, Wang Y (2009) J Mol Struct (Theochem) 899:111